

石崎忠彦・岩谷隆一・中北地獄山資料センターデータベース化研究グループ (2008) 地震・噴火史料データベース (年代・中北編) のインターネット公開.

日本地質学連合大会. Mansinha, L. and Smylie, D. E. (1971) The displacement fields of inclined faults. Bull. Seism. Soc. Am., 61, 1433-1440.

Minoura, K. and Nakaya, S. (1991) Traces of tsunami preserved in intertidal lacustrine and marsh deposits: some examples from northeast Japan. J. Geology, 99, 365-387.

Minoura, K., Imamura, F., Sugawara, D., Koito, Y. and Iwashita, T. (2001) The 869 Jogan tsunami deposit and recurrence interval of large-scale tsunami on the Pacific coast of northeast Japan. J. Natural Disaster Sci., 23, 83-88.

佐竹健治・山本 浩・山本 浩 (2003) 17世紀に北前道五部で発生した異常な津波の震源モデル. 佐竹健治・山本浩・佐竹健治 3, 315-362.

佐竹健治・岡村行信・岩谷隆一・津浦孝夫・Than Tin Aung・小松原純子・藤井謙一郎 (2006) 佐竹健治の津波研究に記録された歴史時代の巨大津波. 地質学雑誌, 624, 36-41.

佐竹健治・岩谷隆一・岡村行信・山田宗太・佐藤孝夫・Than Tin Aung・小松原純子・藤井謙一郎・藤原治・佐竹健治・津浦孝夫・佐藤健治 (2007) シンディ・オオノスライカーを用いた岩谷隆一・山田宗太・佐藤孝夫・佐藤健治・佐藤健治・佐藤健治 (2007) における津波伝播経路. 佐竹健治・佐藤健治研究報告, No. 7, 47-80.

江川祐祐・岩谷隆一・小松原純子 (2008) ハンドブックを用いた岩谷隆一・山田宗太・佐藤健治・佐藤健治・佐藤健治 (2008) における津波伝播経路. 佐竹健治・佐藤健治研究報告, No. 8, 17-70.

Sawai, Y., Fujii, Y., Fujiwara, O., Kamataki, T., Komatsubara, J., Okamura, Y., Satake, K. and Shikimaru, M. (2008) Marine incursions of the past 1500 years and evidence of tsunamis at Suji-numa, a coastal lake facing the Japan Trench. The Holocene, 18, 517-528.

岩谷隆一・佐竹健治・岡村行信・小松原純子・Than Tin Aung・石山忠也・岩谷隆一・藤井謙一郎 (2007) 佐竹健治の津波研究報告, No. 7, 31-46.

岩谷隆一・佐竹健治・佐藤健治 (2001) 西暦 869 年 佐竹健治による津波作用とその伝播経路. 津波工学研究報告, 18, 1-10.

佐竹健治 (1998) 日本津波伝播経路【第2版】. 東京大学出版会, 238 pp.

佐竹健治 (1998) 869 (貞観 11) 年の地震・津波の伝播経路. 佐竹健治の津波研究, 歴史地理, 14, 83-99.

佐竹健治 (2000) 貞観十一年 (869 年) 地震・津波と推定される津波の伝播経路 (総論). 歴史地理, 16, 59-77.

佐竹健治 (2001) 佐竹健治の地震・津波の伝播経路. 佐竹健治の津波研究, 歴史地理, 17, 130-146.

(交付: 2008 年 8 月 31 日. 受理: 2008 年 10 月 18 日)

Table 1. Parameters of fault models examined in this study.

Table with 10 columns: Model, Fault type, Depth (km), Dip (deg), Strike (deg), Dip (deg), Rate (deg), Slip (m), Mw, M0 (Nm). Rows include Normal Fault, Tsunami Eq., d15W50, d31W20, d15W100, d31W100, d31L100d10, Sendai Bay Fault, and d15W100b7.

佐竹健治・岩谷隆一・山本浩・山本浩 (2003) 17世紀に北前道五部で発生した異常な津波の震源モデル. 佐竹健治・山本浩・佐竹健治 3, 315-362.

Table 2. Inundation distances (in km) along profiles computed for ten models of the Jogan tsunami, compared with the location of the most inland tsunami deposits.

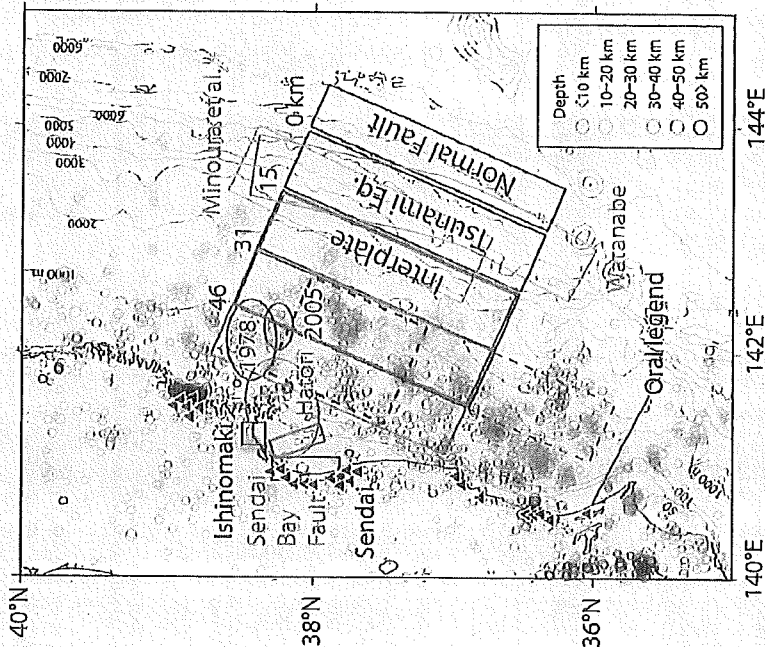
Table with 10 columns: Tsunami deposit, Model 1 Normal Fault, Model 2 Tsunami Eq., Model 3 d15W50, Model 4 d31W50, Model 5 d15W100, Model 6 d31W100, Model 7 d31L100d10, Model 8 d31W100b7, Model 9 Sendai Bay Fault, Model 10 d15W100b7. Rows include bhinomaki, WA, AJ, Y, Sendai, a, b, c, d, e.

The lowest two lines indicate averages and standard deviations of distance ratio (formulated inundation distance / tsunami deposit from eqn). Both rank A and B deposits are included in the calculations. The averages and standard deviations shown in bold are the preferred models.

第3表. 10 (M07) 型プレートモデルを用いた最内帯津波堆積物の高さ (m) との比較
 Table 3. The water heights (in meters) along profiles computed for ten models of the Jogan tsunami, compared with the altitudes (in meters) of the most inland tsunami deposits.

Tsunami deposit	Model 1	Model 2	Model 3	Model 4	Model 5	Model 6	Model 7	Model 8	Model 9	Model 10
	Normal Fault	Tsunami Eq.	d15W50	d1W50	d15W100	d1W100	d15L200	d1L200	Sendai Bay Fault	d15W1000
Ishinomaki										
WA	1.9	1.7	2.0	2.2	2.4	2.0	2.1	2.7	2.4	3.6
A1	1.7	1.8	2.1	0.7	0.8	1.1	1.2	1.9	1.6	1.7
Y	2.0	1.8	2.1	2.1	1.9	2.4	2.1	2.5	1.4	2.5
Sendai										
a	2.0	2.0	1.1	1.6	1.4	1.7	1.3	2.4	2.2	2.4
b	3.3	2.2	1.1	1.5	1.6	1.7	1.3	2.5	2.2	2.5
c	2.5	1.8	0.9	1.2	1.0	1.3	1.4	2.0	2.0	2.1
d	3.0	1.0	1.1	1.9	2.0	2.3	2.5	3.5	1.3	3.2
e	3.9	1.7	2.1	3.0	2.7	3.1	3.0	2.7	4.0	4.1
Height ratio	Average	0.72	0.65	0.68	0.64	0.78	0.66	1.04	0.78	1.09
Stnd. Dev.	Std. Dev.	0.26	0.35	0.25	0.25	0.17	0.22	0.21	0.29	0.24

The last two lines indicate averages and standard deviations of height ratio (simulated inundation height / altitude of the most inland tsunami deposit). Both rank A and B deposits are included in the calculations. The averages and standard deviations shown in bold are the preferred models.



第1表. 10 (M07) 型プレートモデルを用いた最内帯津波堆積物の高さ (m) との比較
 Table 3. The water heights (in meters) along profiles computed for ten models of the Jogan tsunami, compared with the altitudes (in meters) of the most inland tsunami deposits.

Figure 1. Fault models of the Jogan tsunami. The fault models tested in this study are the normal fault, tsunami earthquake and interplate earthquake models (widths: 30 km (shown by black solid lines), interplate models with different fault length (shown by black dashed lines), with different fault widths (green and blue lines), and an active fault in Sendai Bay (dark green). In addition, those proposed by Hatori (1998), Watanabe (2000) and Minoura et al. (2001) are shown. The source areas of 1978 and 2005 Mito-oki earthquakes are also shown. Color circles indicate seismicity in this region between October 1997 and March 2007, according to Japan Meteorological Agency data. Numerals beside the faults (0, 15, 31, and 46) indicate upper depth of the faults. Triangles show localities where oral legends of the 869 Jogan earthquake and tsunami were reported (Watanabe, 2000).

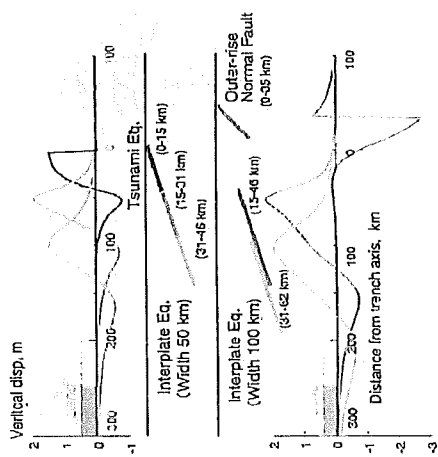


Fig. 2. Vertical seafloor deformation due to outer-rise normal fault, tsunami earthquake and interplate earthquakes with different fault width and depth. Gray rectangles and broken lines indicate location of land on the head of Sendai bay, and Ojika Peninsula, respectively.

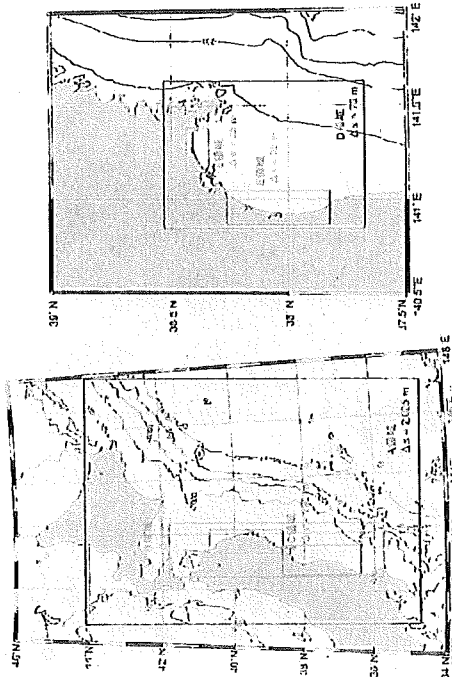


Fig. 3. Computational grids for tsunami numerical simulation. Grid sizes are 2,025 m, 675 m, 225 m, 75 m, 25 m, 25 m, 25 m, 25 m, 25 m, and 25 m; smaller grids are used near coasts.

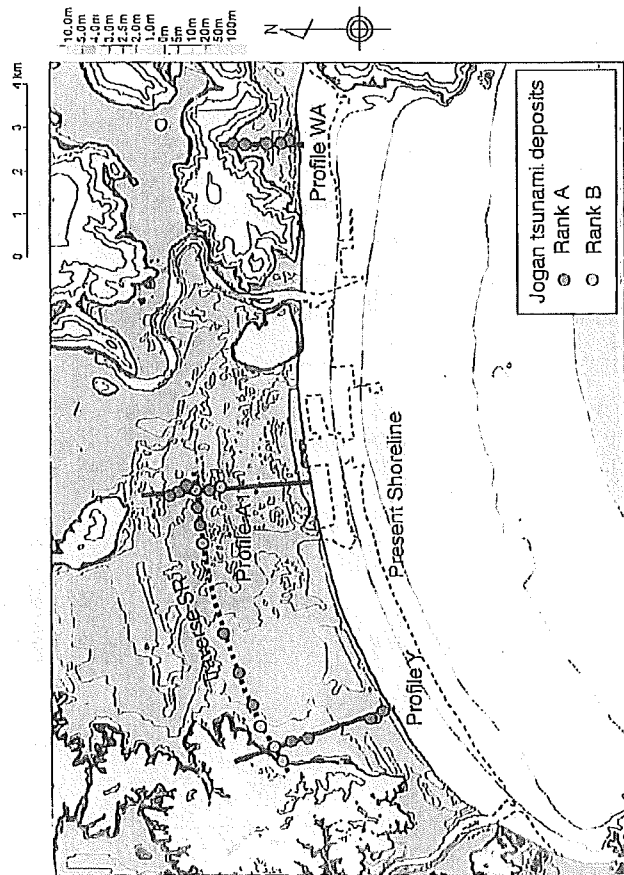
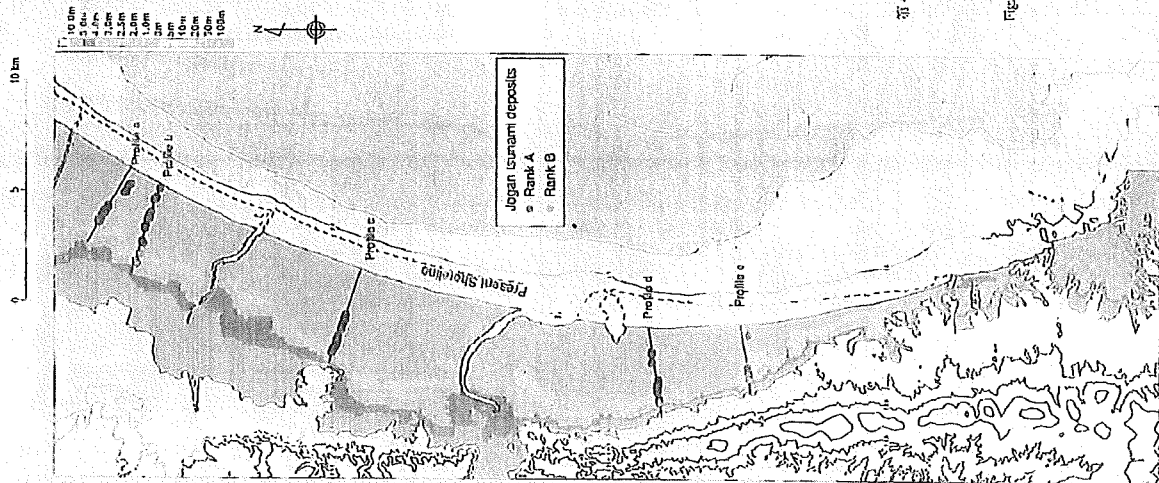
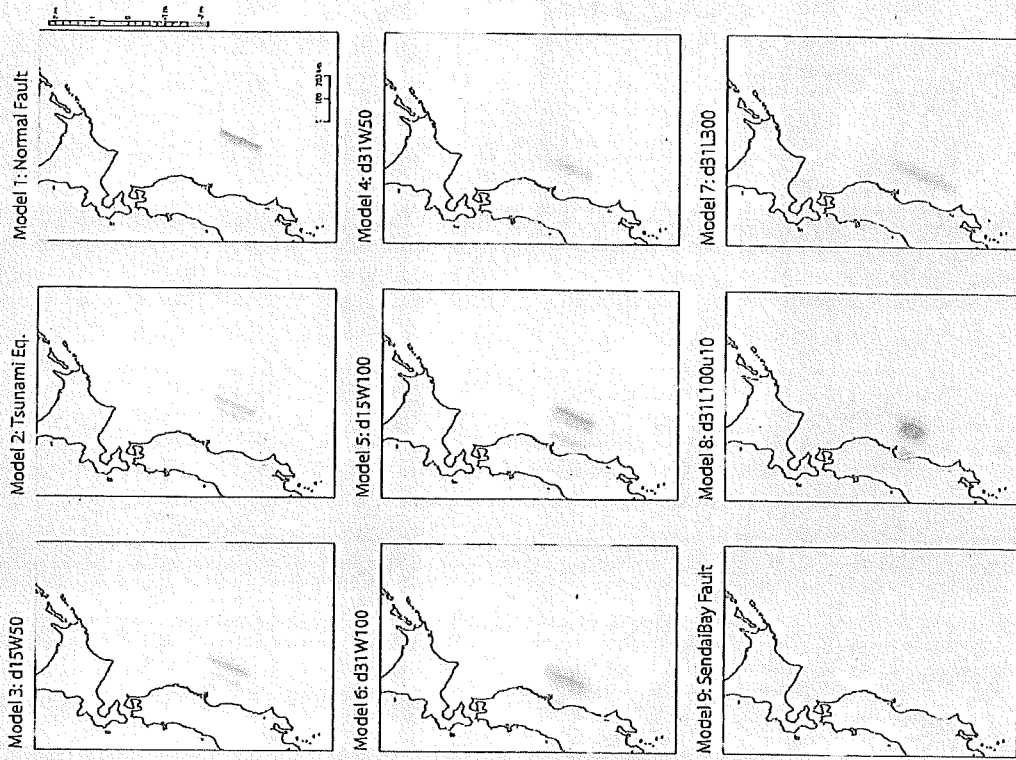


Fig. 4. Estimated topography of Ishinomaki plain at the time of AD 869 Jogan tsunami. This area is gridded into 25 m interval for inundation modeling. Locations of the tsunami deposits (Shishikura et al., 2007) and three profiles on which simulation results are compared with the deposits are shown. Ranks A and B refer to probability of the Jogan tsunami deposits.



第46図 前巻の佐竹町市周辺の地形図(標高10mから25m). 佐竹町市が現在から約10km西にあり(佐竹町市は2007, 2008) 佐竹町市は佐竹町市と佐竹町市との間にあり(佐竹町市は2007, 2008) 佐竹町市は佐竹町市と佐竹町市との間にあり(佐竹町市は2007, 2008) 佐竹町市は佐竹町市と佐竹町市との間にあり(佐竹町市は2007, 2008)

Fig. 46. Estimation topography around Sendai plain at the time of AD 869 Jogan tsunami. This area is gridded into 25 m interval for inundation modeling. Locations of the tsunami deposits (Sawai et al., 2007, 2008) and five profiles on which simulation results are compared with the deposits are shown. Ranks A and B refer to probability of the Jogan tsunami deposits



第5図 佐竹町市・佐竹町・山本 区 佐竹町市周辺の地形図(標高10mから25m). 佐竹町市が現在から約10km西にあり(佐竹町市は2007, 2008) 佐竹町市は佐竹町市と佐竹町市との間にあり(佐竹町市は2007, 2008) 佐竹町市は佐竹町市と佐竹町市との間にあり(佐竹町市は2007, 2008)

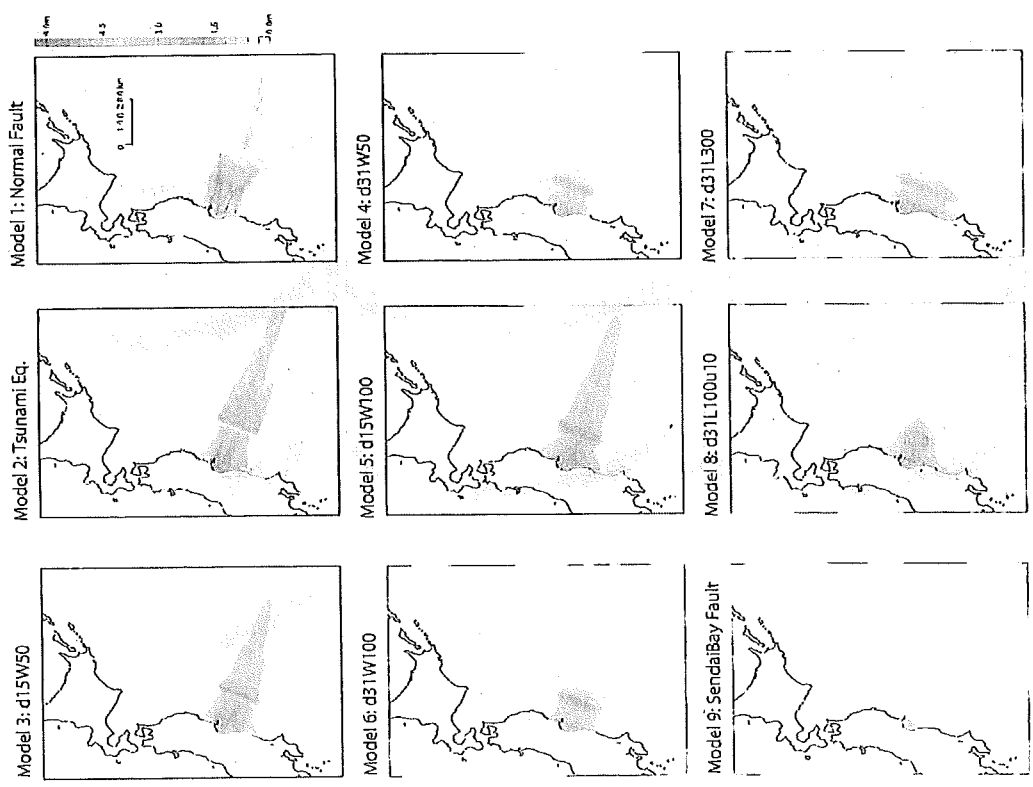


図 6 佐竹直志・竹谷洋一・山本 雄による佐竹直志らの研究 (2005) の結果を基に、モデル 1-9 の最大海面変動を示した。モデル 10 はモデル 5 とほぼ同じパターンを示した。
 Fig. 6. Maximum sea surface displacements for models 1-9. Model 10 is not shown because its pattern is almost same as that of d15W100 (model 5).

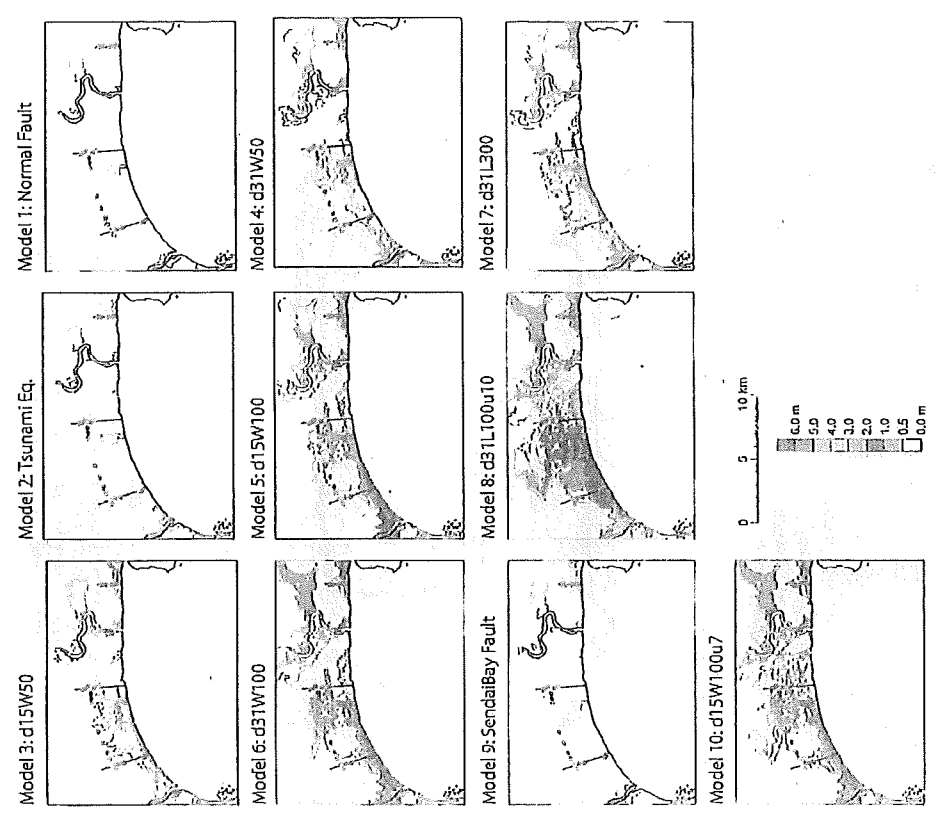


図 7 佐竹直志・竹谷洋一・山本 雄による佐竹直志らの研究 (2005) の結果を基に、モデル 1-10 の最大水深を示した。図 4a, 図 4b, 図 4c。
 Fig. 7. Maximum flow depth computed for models 1-10 and distribution of tsunami deposits (red or blue circles; see fig. 4a) in the Ishinomaki plain.

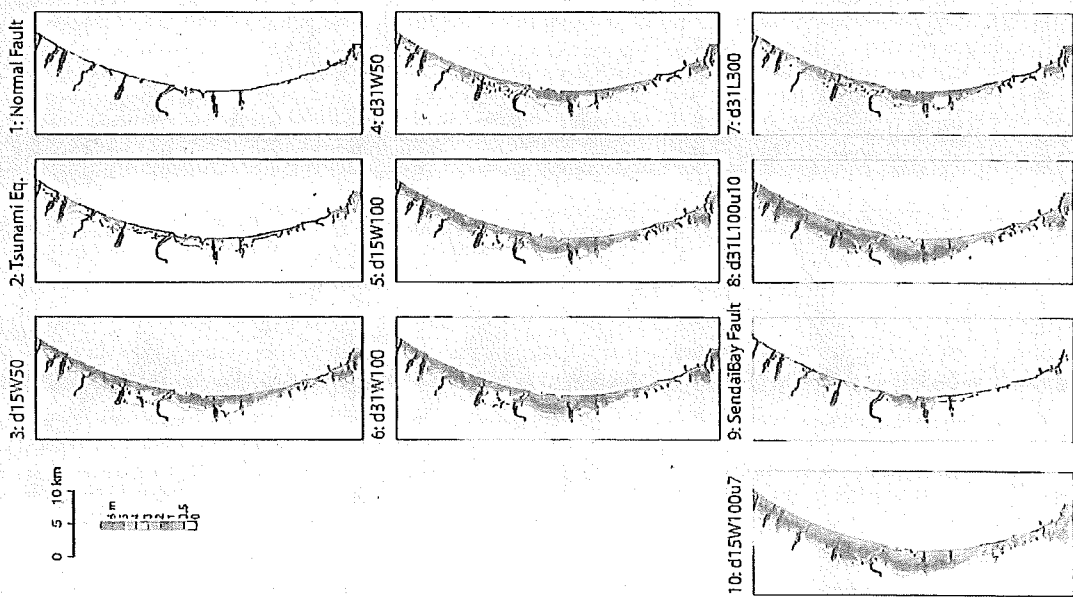


図 8. 最大流量深さ (m) の分布 (モデル 1-10) の比較 (佐藤・山本・山本 2007).
 Fig. 8. Maximum flow depths computed for models 1-10 and distribution of tsunami deposits (red or blue circles; see Fig. 4b) in the Sendai plain.

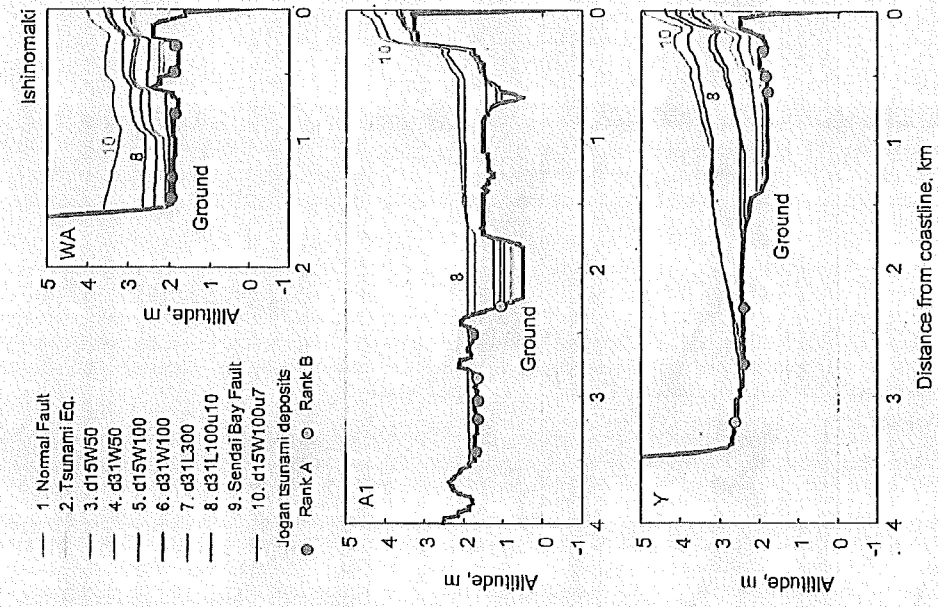


図 9a. 石巻平野の地形・地質・地質学的な特徴とその成因 (佐藤・山本・山本 2007).
 Fig. 9a. Profiles of topography and maximum water surfaces along three profiles in the Ishinomaki plain. Distribution of tsunami deposits (Fig. 4a; Shikama *et al.*, 2007) are also shown.

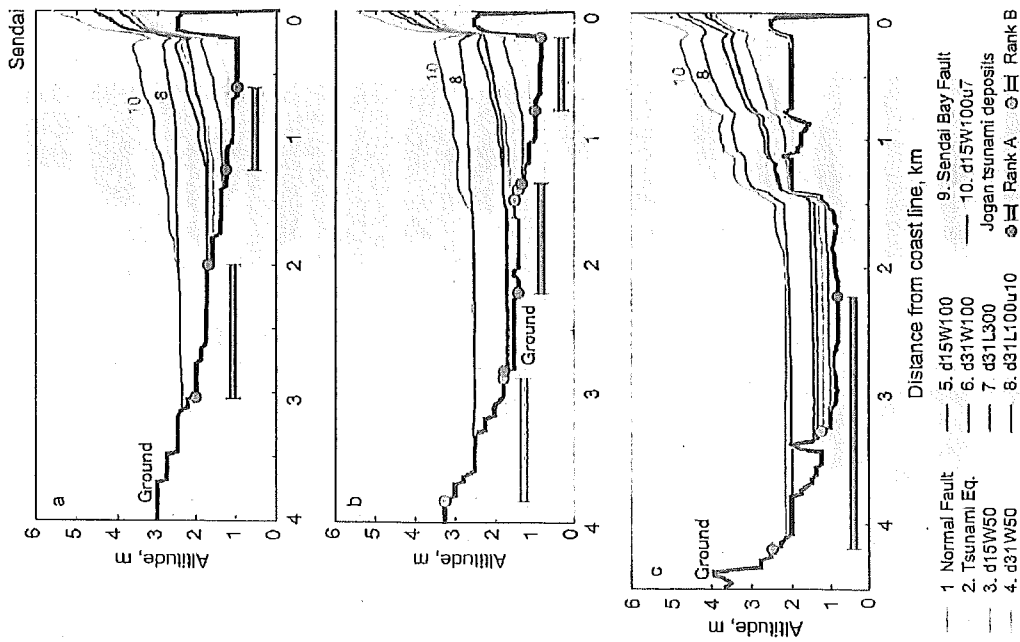


図 9b. 仙台平野の 3 個の異なる地形・津波水位断面図。津波堆積物の分布 (第 4b 図、第 4c 図、第 4d 図、第 4e 図、第 4f 図、第 4g 図、第 4h 図、第 4i 図、第 4j 図、第 4k 図、第 4l 図、第 4m 図、第 4n 図、第 4o 図、第 4p 図、第 4q 図、第 4r 図、第 4s 図、第 4t 図、第 4u 図、第 4v 図、第 4w 図、第 4x 図、第 4y 図、第 4z 図) は、それぞれ異なる地形・津波水位断面図を用いて示されている。図 9c. Profiles of topography and tsunami maximum water surface along three profiles in the Sendai plain. Distribution of tsunami deposit (Fig. 4b, Sawai *et al.*, 2007; 2008) are also shown.

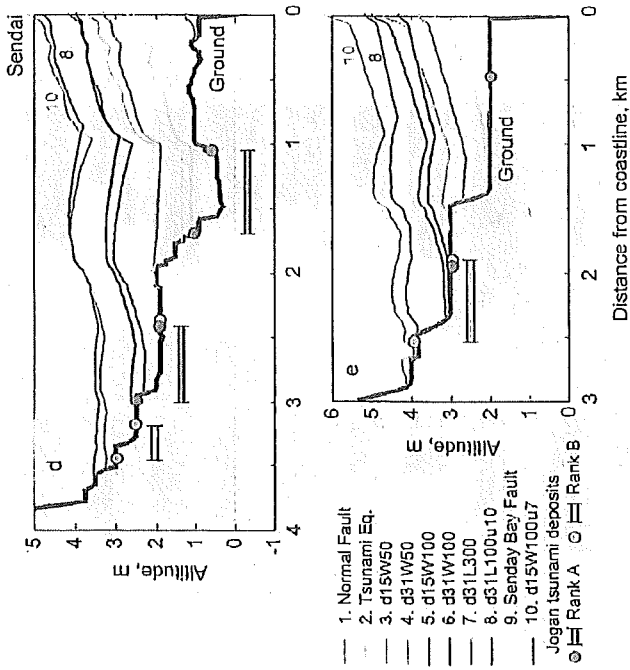


図 9c. 仙台平野の 2 個の異なる地形・津波水位断面図。津波堆積物の分布 (第 4b 図、第 4c 図、第 4d 図、第 4e 図、第 4f 図、第 4g 図、第 4h 図、第 4i 図、第 4j 図、第 4k 図、第 4l 図、第 4m 図、第 4n 図、第 4o 図、第 4p 図、第 4q 図、第 4r 図、第 4s 図、第 4t 図、第 4u 図、第 4v 図、第 4w 図、第 4x 図、第 4y 図、第 4z 図) は、それぞれ異なる地形・津波水位断面図を用いて示されている。図 9c. Profiles of topography and tsunami maximum water surface along 2 files in the Sendai plain. Distribution of tsunami deposit (Fig. 4b, Sawai *et al.*, 2007; 2008) are also shown.

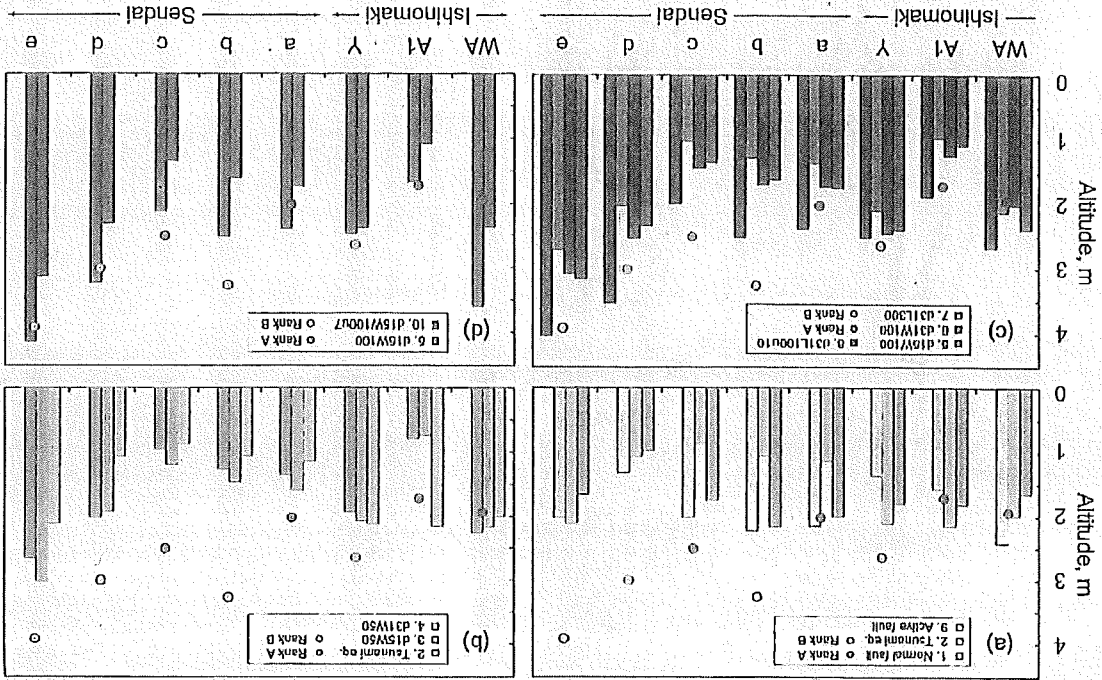


Fig. 11. Comparison of rump heights and location of the most inland tsunami deposits along eight profiles in the Ishinomaki and Sendai plains.

図 11 伊勢・仙台平野の 8 断面の津波堆積物の位置と堆積面の比較

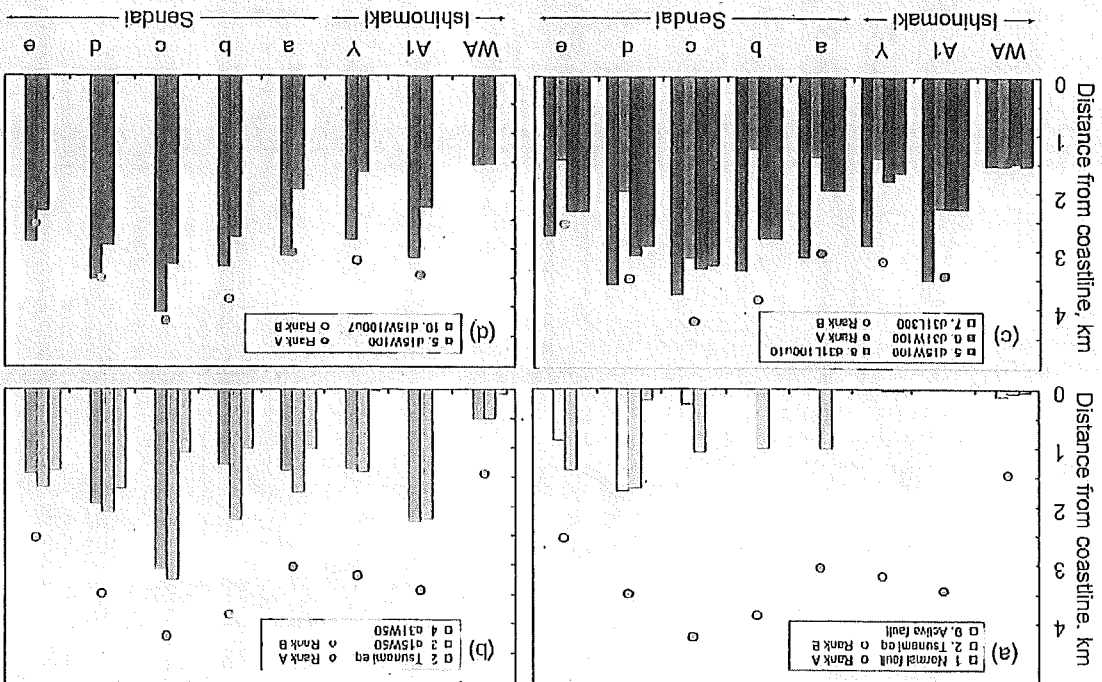


Fig. 10. Comparison of foundation distance and location of the most inland tsunami deposits along eight profiles in the Ishinomaki and Sendai plains.

図 10 伊勢・仙台平野の 8 断面の津波堆積物の位置と基礎距離の比較